# Uniform Manifold Approximation and Projection as Anomaly Detection Applied to Masking Scenarios of Plutonium

Marcus J. Neuer[1,2] and Elmar Jacobs[1]

[1] innoRIID GmbH, Merowingerstr. 1, 40237 Duesseldorf, Germany, http://www.innoriid.eu
[2] RWTH Aachen,Turmstr. 46, 52064 Aachen, Germany, http://www.rwth.de

**Abstract.** Unsupervised learning strategies have proven successful for detecting anomalies in various applications. UMAP, the uniform manifold approximation and projection technique, is a transformation that maps complex input data to a reduced dimensional map. It is applied to real-world spectral data of Plutonium, measured with Sodium Iodide (NaI:Tl), Lanthanum Bromide (LaBr3:Ce,Sr) and Cadmium Zinc Telluride (CZT) detectors. Through the manifold mapping, similar spectral structures are clustered while anomalies are highlighted by a different position in the reduced dimensional subspace. In addition, the simpler t-Student Neighbour Embedding algorithm is used on the same data for comparison with UMAP.
The paper shows further geometric strategies to provide reproducible results with the mapping and physics-informed learning algorithms that implement existing UMAP and t-SNE techniques in a forward prediction of the spectroscopic scenario. Data from real-world tests involving Plutonium and medical nuclides like Iodine I-131 is tested and evaluated with this forward prediction. Also naturally occurring masks like K-40 are considered and discussed.

**Keywords:** machine learning, uncertainty quantification, stochastic dynamics

## 1 Introduction

Discrimination of threat material against innocent source one of the tasks of nuclear detection equipment. Spectral signatures are one basis for this. The inherent energetic imprint of gamma particles from the source is measured with a radiation detector. Ranging from medium to highly resolving techniques, homeland security applies a diversity of different instruments, but those are based on two mayor technological types o: scintillators and semiconductors. Where semi-conductors like Cadmium-Zinc-Tellurite (CZT) and high-purity

Germanium (HPGe) yield high resolutions and scintillators like Sodium Iodide (NaI:Tl) or Lanthanum Bromide ($LaBr_3$:Sr,Ce) provide medium resolutions.

A cornerstone for performance is the identification of special nuclear material (SNM) in the presence of masking material. Masks are often medical isotopes with peaks close to the SNM or radiation activities high enough, to shield effectively any other source. In the present paper, we concentrate on the separation of Weapon-Grade Plutonium (WGPu) and Iodine (I-131).

Starting point of the analysis are spectra that we gathered in numerous data taking campaigns, from which we derived several base spectra for internal algorithm development. We utilize a Monte-Carlo code to actually generate a homogeneous mix of training spectra for a machine learning evaluation.

Among the discipline of machine learning and data analytics, one distinguishes supervised and unsupervised methods. While supervised methods know the training targets – the so-called labels – for their predictions, unsupervised learning only works with the data itself [1]. It tries to find structures and categories, that can help to classify the data in an automatic way. The classification is normally done by a secondary (often supervised) algorithm.

In the course of this work, we will apply clustering algorithms to the separation problem of Iodine and WGPu. More specifically, we will apply the t-Student Distributed Stochastic Neighbour Embedding (t-SNE) which was extensively discussed by Maaten et al. [2], [3]. We will use t-SNE as an explanatory technique and then extend our treatment to the Uniform Manifold Approximation and Projection (UMAP) as presented by McInnes et al. in 2018 [4]. These methods have longstanding success in the ML community. They showed reasonable success in diverse industrial problems, among which [5] is only one example.

## 2 Problem statement and measurement data

### 2.1 Masking

Masking scenarios play a tremendous role in homeland security applications. Nuclear threats that are masked by harmless isotopes pose a threat to society and should be detected in a reliable way. Typically such evaluations are done by spectroscopic experts. They analyse the spectrum, compare it to common line catalogues and determine the nature of the source. In recent years, automatic nuclide identification has matured. It supports the work of these experts and provides a first, quick on-site evaluation of the spectra. Often this result triggers secondary and tertiary actions according to security protocols. Consequently, it is important to develop algorithms that have good performance in distinguishing innocent and threat sources.

### 2.2 Spectral data of the masking scenario

We use different WGPu and Iodine measurements with known activities. These measured spectra are stored in N42 files and have clear provenance, that means we know exactly where these measurements were acquired, under which circumstances and especially, which type of source was present. These data are our ground truth. All spectra have also be obtained with a sufficient statistics ($> 10^6$ counts). The spectra are denoted with the symbol $\mu$ and we say that a data set of $\mu_i$ comprises a certain number of $M$ spectra, so that $i$ numbers each individual spectrum.

We also consider three different detector materials: NaI:Tl, $LaBr_3$:Ce,Cr and Cadmium Zinc Telluride (CZT), where the first two are scintillation detectors and CZT is a semiconductor. There are many differences among those detectors, where the most prominent one is their resolution in terms of full-width-at-half-maximum (FWHM). NaI:Tl has by far the lowest resolution, with 6% to 8% at the Cs-137 line with 661.65keV. In contrast, $LaBr_3$:Ce,Sr yields 3% or better and CZT even reaches resolutions below 2%. For most of the remaining description, we will remain with NaI:Tl spectra, without limiting the generality of the method. The other two detectors will be discussed in the results section.

Figure 1 shows assorted NaI:Tl spectra for WGPu + I-131 mixtures at different ratios, starting with pure Iodine and leading towards a 50% mixture of both. Note, we will restrict to these minimum (0% WGPu) and maximum (50% WGpu, 50% I-131) ratios throughout of our work.

### 2.3 Data extension with Monte-Carlo casting

As we need large data sets for the training, we use a Monte-Carlo approach for extending the actual data set. The procedure that we use takes the measured spectrum $\mu$ as a probability distribution and then casts random samples from this distribution. We are free in our choice of the number of these samples. So, once we have longterm measurements that contain spectral data of multiple minutes, we can still use this technique to reduce the data down to a fixed number of counts. As a total number of $30k$ counts per spectrum is reasonable for our applications, we stick with the number. Considering again Fig. 1, we generate all relevant mixtures ratios where we have not measurements.

## 3 Unsupervised manifold mapping techniques

### 3.1 Data normalisation prior to mapping

Before we discuss the mapping procedures, we focus on the data preparation. For the success of our technique, it is important to exclude any characteristics that originates from counts

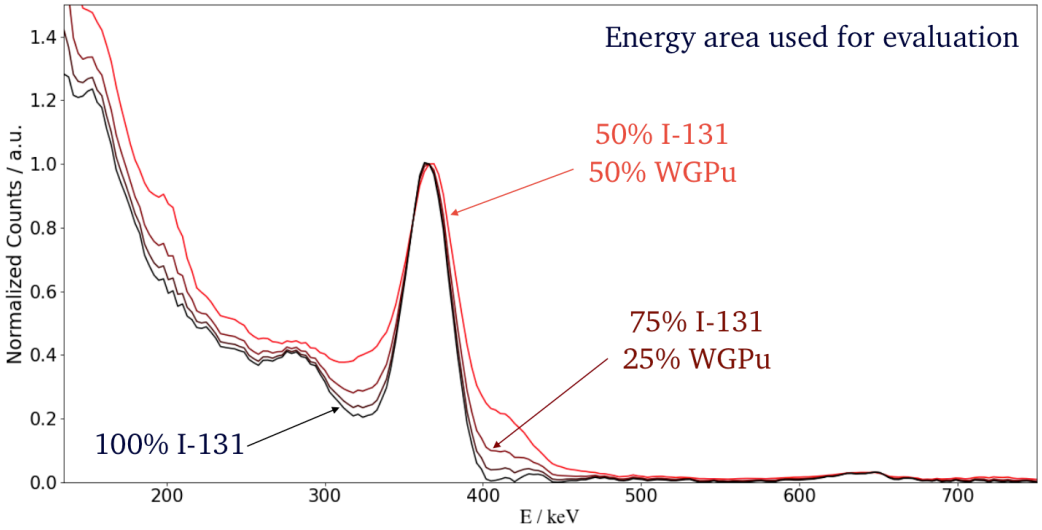


Fig. 1: Assorted NaI:Tl spectra of our training set. Shown are different mixture ratios of I-131 and WGPu, with a stronger red color for increasing WGPu amounts. All spectra are normalised to maximum of the I-131 peak. Detector size was $3'' \times 1''$.

or positioning of the spectrum itself. Therefore we normalise each spectrum to the counts of the Iodine peak at 364keV. All relevant WGPu structures for the discussed technique are located around this peak. After normalisation, we also subtract the mean of the spectrum by the following process:

$$\mu \mapsto \mu - \langle \mu \rangle, \tag{1}$$

where $\langle \mu \rangle$ is the expectation value of $\mu$.

### 3.2 t-Distributed Stochastic Neighbour Embedding

Let us first review the idea behind t-SNE. It allows us to understand the mechanism behind projection techniques in a bit detail. We will transfer the common nomenclature from unsupervised learning directly into the spectroscopy language, to ease the understanding of the theory. First, we start with our data space $\Omega$ in which we have data vectors $\mu_i \in \Omega$. Imagine $\Omega$ to be $\Omega = \mathbb{R}^N$ with a dimension of $N = 1024$ for the course of this work, as this is a feasible example for a space that represents spectrum measurements. Consequently, each $\mu$ represents a spectrum with 1024 channels. Note, for our later evaluation, not all 1024

channels are used, but only a subset. Lowering the amount of data of course speeds up the algorithm performance.

The next steps helps to identify the neighbourhood of two spectra:

**Definition 1 (Gaussian neighbourhood).** *Let $x_i$ and $x_j$ be two spectra defined in $\Omega$. We define the probability $p(i|j)$*

$$p(i|j) = \frac{1}{\sum_{k\neq i} \exp\left[-\frac{||x_i - x_k||^2}{2\sigma^2}\right]} \exp\left[-\frac{||x_i - x_j||^2}{2\sigma^2}\right]. \tag{2}$$

*that quantifies the chance that $x_j$ is indeed a neighbour of $x_i$.*

In our data, we can use Eq. 2 to find $p(i|j)$ for all tuples $(x_i, x_j)$, which takes some time, as we have to iterate through all individual data points. $p(i|j)$ tells us, how similar these spectra are. The operation $||.||$ can be any p-norm $||x|| = (\sum_i |x_i|^p)^{1/p}$ on $\Omega$, but we choose here $p = 1$, the 1-norm.

We now consider a second space $\Xi$, e.g. with $\Xi = \mathbb{R}^2$ with elements of $\Xi$ being denoted as $y_i \in \Xi$. For each data point $x_i \in \Omega$ there should be a associated data point $y_i \in \Xi$ and the association between $x_i$ and $y_i$ is bijective.

**Theorem 1 (t-SNE Algorithm).**

*Given a series of data points $x_i$ in a space $\Omega$, the t-SNE procedure determines a series of associated data points $y_i$ in a lower dimensional space $\Xi$, by optimizing the Kullback-Leibler divergence,*

$$KL(p, q) = \sum p(i|j) \log \frac{p(i|j)}{q(i|j)} \tag{3}$$

*where the Neighbourhood probability $q(i|j)$ for the points in $\Xi$ is given by a t-Student distribution,*

$$\tilde{p}(i|j) = \frac{1}{\sum_l \sum_{l\neq m} \frac{1}{1+||y_l - y_m||^2}} \left[\frac{1}{1 + ||y_i - y_j||^2}\right]. \tag{4}$$

The theorem reflects already the way, t-SNE works. In practise, the first selection of points $y_i$ can be random. Any further modification to the points should consequently lead to a minimization of (3), which is typically done with stochastic gradient decent [6]. Equation (3) is the Kullback-Leibler divergence, which is a well-known measure for the distance between two distributions. When both distributions are equal,

t-SNE has several shortcomings that makes reduces its practical use:

– Its training is not reproducible (only for fixed random seeds)
– The positioning of the clusters is not analytically related to the original data

Yet, t-SNE is very good proof-of-work for this type of analysis and therefore part of this work. We started with t-SNE, exploring the separation potential of spectral data and evaluating the confidence indices associated with this technique. If you fix the random seed and restrict to a single, frozen training state of your t-SNE predictor, algorithmic models obtained with this approach can very well already distinguish the SNM and the masking source.

### 3.3 Uniform Manifold Approximation and Projection (UMAP)

The UMAP procedure is related to t-SNE, in the sense that it also projects the data onto a smaller subspace. Nonetheless, the construction of that space is different. UMAP first constructs a high dimensional graph representation of our data. The edges of this graph are hereby scaled by the probability, how close two points are to each other. Different graph structures, the so-called simplices are used to form simplicial sets. Each singular point is a 0-simplex, each connection of two points is a 1-simplex and connections of 3 points represent a 2-simplex (triangle). This procedure is followed up to higher order simplices.

Lastly this high dimensional representation maps our data topology and by restricting to only the small simplices, we will not loose significant information, as those simplices already contain a predominant part of the topology. With that approach, the high dimensional data is projected onto a space with smaller dimensions. For further details we refer to [4].

The actual training is finally again performed by minimizing (3), respectively with regularized variants of Eq. (3).

## 4 WGPu analysis algorithm based on 2D mapping

### 4.1 2D point cloud evaluation

The outcome of either t-SNE or UMAP training is an unsupervised method that produces 2D point cloud mappings with resulting points $(y_{i,0}, y_{i,1})$ for each input.

**Definition 2 (2D mapping operator).** *We define the 2D-mapping operator $\square_{2D}$ as the projection of a spectrum $\mu \in \mathbb{R}^N$ with $N$ channels onto the 2-dimensional subspace $\Xi$,*

$$\begin{pmatrix} y_0 \\ y_1 \end{pmatrix} = \square_{2D} \left[ \begin{pmatrix} \mu_0 \\ \mu_1 \\ \vdots \\ \mu_N \end{pmatrix} \right]. \tag{5}$$

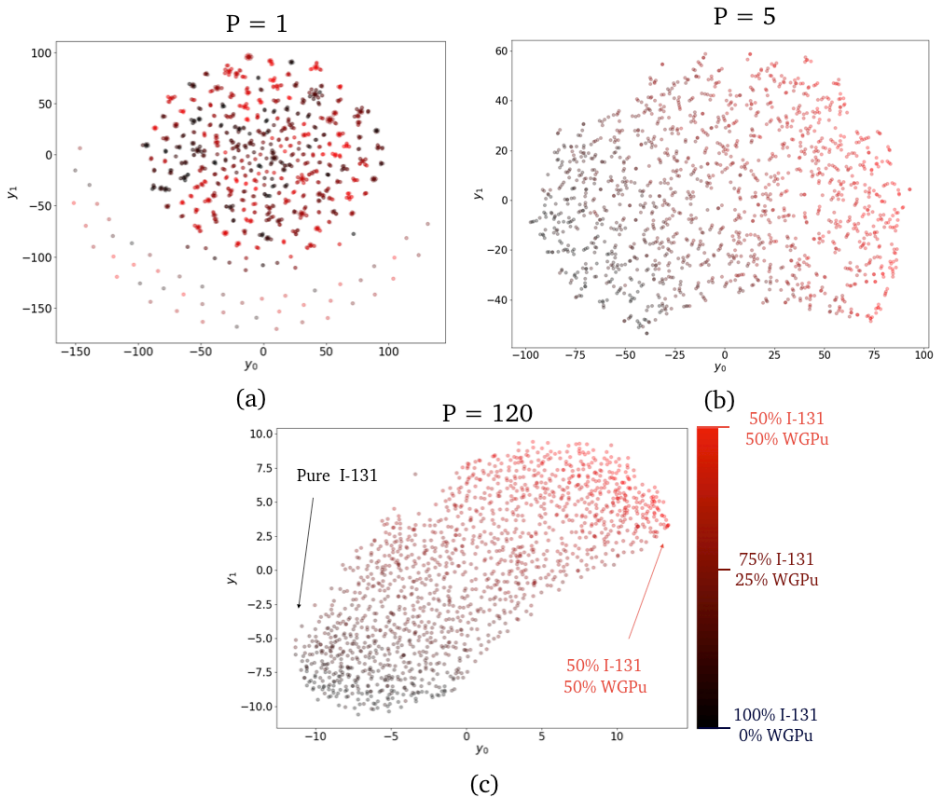


Fig. 2: Applying t-SNE to the training set and visualising the according 2D mapping for different perplexities. For larger $P$, clear distinction between different WGPu / I-131 ratios becomes feasible.

*with* $y = (y_0, y_1) \in \Xi$ *being the mapped transformation of the spectrum.*

Of course, this only formalizes the reason we discussed the two algorithm in the former section. The actual 2D mapping is found with either of these two approaches:

**Lemma 1 (Finding the mapping operator).** *The mapping operator can be established by training either a t-SNE algorithm or a UMAP algorithm.*

### 4.2 Analysis algorithm

First we formally define the quantity, that we would like to determine with our algorithm – namely the output of the WGPu ratio.

**Definition 3 (WGPu ratio).** *The quantity $\varphi$ reflects the amount of plutonium in a normalised spectrum $\mu$.*

Calculating this value from the actual mapping requires an algorithm that receives $(y_0, y_1)$ as input for a subsequent regression. Abstractly, we can define such an algorithm as follows:

**Definition 4 (WGPu quantification algorithm).** *Any regression algorithm $\Phi$, that associates $(y_0, y_1)$ with the WGPu ratio $\varphi$ is called WGPu quantification algorithm and evaluated according to*

$$\varphi = \Phi(y_0, y_1) = \Phi[\square_{2D}(\mu)]. \tag{6}$$

With the above approach, we assume that this mapping conserves the inherent differences of the spectra and renders them into a space, where we can distinguish mixtures better than in the original spectrum. Practically, we put a test spectrum into the trained function (5) and end up with two numerical values that are coordinates on the map. If the resulting point is close to those points representing a specific amount of WGPu, we associate this value with our measurement. This last association task can be done with various supporting regression procedures, such as decision trees, neural nets or geometric regressors. In our case we use a neural network as practical realisation:

**Lemma 2 (Practical realisation of $\Phi$).** *The algorithm $\Phi$ can be obtained by training a neural network with the topology $[2, q_1, q_2, ..., q_L, 1]$, where $L$ is the number of layers. In practise, a layer size of $L = 2$ is sufficient for good results.*

## 5 Results

### 5.1 Training and test data

We split the data manually into training and test data. This can be done also with cross-validation techniques. In the present case, training data consisted of 1500 spectra determined as described in Sec. 2. The test data contains 500 different spectra, with similar ratios $\varphi$.

The t-SNE algorithm was trained and the results of the t-SNE transformed spectra are shown in Fig. 2. Here, different hyperparameter values for the perplexity are used, ranging from $P = 1$ to $P = 120$. Note that the capability of separating I-131 and WGPu increases with the perplexity.

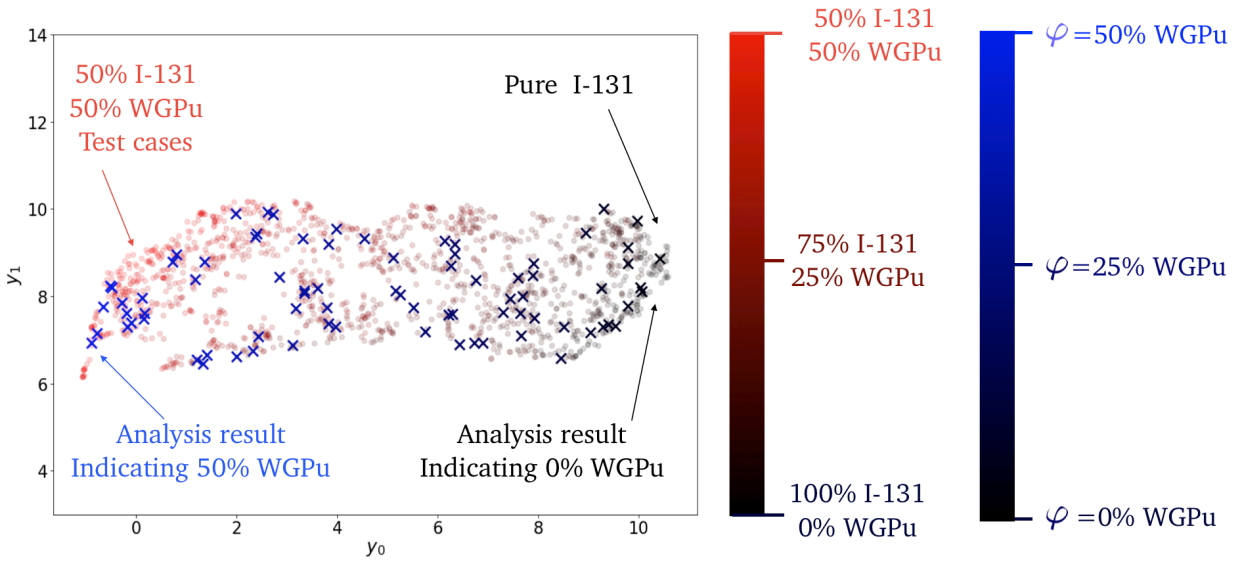


Fig. 3: UMAP result (red-black gradient) and derived analysis algorithm result (blue-black gradient). Blue crosses indicate the results of the WGPu ratio quantisation algorithm.

## 5.2 UMAP

Fig. 3 shows the point clouds for our training spectra, now using the UMAP technique. The separation quality is better than with t-SNE, as one can see from the stretching of the data points in $\Xi$ (the whole 2D area of the diagram).

## 5.3 WGPu ratio quantisation

Based on the point clouds derived with the UMAP technique, we coupled a neural network to the output of UMAP, as described in Lemma 2. This neural network is tasked to provide the regression between the points $(y_0, y_1)$ and the WGPu ratio $\varphi$ . In the diagrams 1, 2 and 3 this ratio is denoted by the color of a point. The colorbars in 2 and 3 reflect this, too.

We tested the neural network now on the test data – data that was never used for the training. The results of this prediction is also included in Fig. 3 as blue crosses. The blue color scale is similar like the red one. The brighter the color, the higher the predicted value of $\varphi$. The $\varphi$ predictions are plotted directly into the UMAP point cloud. One can see, that the prediction algorithm works well and it determines the value of the WGPu ratio.

### 5.4 Lanthanum-Bromide (LaBr3:Ce,Sr) and Cadmium-Zinc-Telluride (CZT) detector systems

## 6 Summary

An algorithmic way for determining the ratio of WGPu is shown, when it is masked by I-131. Based upon a series of ground truth measurements, an extended data set was obtained with Monte-Carlo methods. This filled up missing ratios and provided a continuous scale of mixtures of both materials. We carefully divided the data set into two groups, a training set and a test set.

The training set was then used to train a t-SNE and a UMAP technique, two mapping approaches that can reduce the dimensionality of the data input onto smaller dimensions, specifically to 2D maps. In this 2D maps, the most important differences of the input data are emphasized and better visible than in the original data.

Once the mapping procedure was in place, a subsequent analysis algorithm was proposed. In the given case, we trained a neural network for coping with the regression problem to relate the map coordinates of t-SNE and UMAP, to a concise value for the WGPu ratio.

Our results indicate, that the separation works well. The prediction algorithm is capable to calculate the right amount of ratio WGPu when masked with I-131. The algorithm can further

## References

1. G. E. Hinton, "Learning multiple layers of representation," 2007.
2. L. J. P. Maaten and G. E. Hinton, "Visualizing high-dimensionality data using t-sne," *Journal of Machine Learning Research*, vol. 9, pp. 2579–2605, Sept. 2008.
3. L. J. P. Maaten and G. E. Hinton, "Accelerating t-sne using tree-based algorithms," *Journal of Machine Learning Research*, vol. 15, pp. 3221–3245, Oct. 2014.
4. L. McInnes and J. Healy, "Umap: Uniform manifold approximation and projection for dimension reduction," *ArXiv*, vol. abs/1802.03426, 2018.
5. M. J. Neuer, A. Quick, T. George, and N. Link, "Anomaly and causality analysis in process data streams using machine learning with specialized eigenspace topologies,"
6. J. Duchi, E. Hazan, and Y. Singer, "Adaptive subgradient methods for online learning and stochastic optimization," *Journal of Machine Learning Research*, vol. 12, no. Jul, pp. 2121–2159, 2011.